

Application of SDRE to Achieve Gait Control in a Bipedal Robot for Knee-Type Exoskeleton Testing

Ping-Kong Huang¹, Chien-Wu Lan¹, and Chin-Tien Wu²

Abstract—Exoskeletons are widely used in rehabilitation and industrial applications to assist human motion. However, direct human testing poses risks due to possible exoskeleton malfunctions and inconsistent movement replication. To provide a safer and more repeatable testing environment, this study employs a bipedal robot platform to reproduce human gait, allowing for controlled exoskeleton evaluations. A control strategy based on the State-Dependent Riccati Equation (SDRE) is formulated to achieve optimal torque control for accurate gait replication. The bipedal robot dynamics are represented using double pendulum model, where SDRE-optimized control inputs minimize deviations from human motion trajectories. To align with motor behavior constraints, a parameterized control method is introduced to simplify the control process while effectively replicating human gait. The proposed approach initially adopts a ramping trapezoidal velocity model, which is then adapted into a piecewise linear velocity-time representation through motor command overwriting. This modification enables finer control over gait phase transitions while ensuring compatibility with motor dynamics. The corresponding cost function optimizes the control parameters to minimize errors in joint angles, velocities, and torques relative to SDRE control result. By structuring velocity transitions in accordance with motor limitations, the method reduce the computational load associated with real-time control. Experimental results verify the feasibility of the proposed parameterized control method in reproducing human gait. The bipedal robot platform provides a reliable and repeatable testing mechanism for knee-type exoskeletons, offering insights into exoskeleton performance under controlled conditions.

I. INTRODUCTION

Exoskeleton robot systems are designed to enhance human muscular strength by utilizing the wearer's movements as control inputs, particularly assisting lower limb activities such as walking. As exoskeleton technology has advanced, its applications have expanded across various fields, including industrial and rehabilitation settings. While these advancements demonstrate the growing potential of exoskeletons in improving mobility and quality of life, practical challenges remain. In particular, for individuals with disabilities, conducting experiments while wearing exoskeletons poses significant risks. For instance, He et al.[19] observed that powered exoskeletons, despite their benefits, carry risks such as malfunctions and inconsistent movement replication, which can compromise safety and reliability. A malfunction or incorrect operation of the exoskeleton could result in irreversible harm to the wearer. Furthermore, the inability to consistently replicate the movements of the wearer during testing introduces substantial variability, which undermines the reliability of the evaluation results.

Previous studies have explored the use of mechanical models. For example, Schrade *et al.* used a mechanical leg

as a test platform to simulate swing phase collisions and compared the collision forces and torques under different stiffness settings, evaluating the effect of knee compliance on collision responses [17]. Laubscher and Sawicki used a PD controller to control a leg model simulating a user with gait disturbances, verifying the gait tracking results of the Gait Guidance Control (GGC) [18].

The mechanical leg model not only provides quantitative evaluation criteria through feedback from sensors but also helps prevent potential injuries during the development process. In addition to providing specific angle commands and using PD control, there are numerous methods in the field of bipedal robot control for controlling mechanical leg models to achieve target movements.

Various approaches have been proposed to improve gait control and energy efficiency. Sanz-Merodio et al. introduced a state-machine-based control method for lower limb orthoses, integrating passive elements such as springs and braking mechanisms to reduce actuator energy consumption, ultimately achieving a 24.6 percentage reduction in energy expenditure [2]. Chen et al. further combined motion intent recognition with dynamic control strategies to address synchronization and stability issues in exoskeleton-assisted walking [3]. Additionally, Tagliamonte et al. validated the feasibility of gait-assistive robots through human-robot interaction experiments, confirming their potential for rehabilitation and mobility enhancement [4].

Shao, Liao, and Cheung [12] optimized the selection of ramp-up time and the ratio of acceleration time to avoid resonance with the system's natural frequency. Reducing vibrations during the operation of the servo motor. Zhu Yu *et al.*[13] proposed a novel approach for tuning the trapezoidal velocity profile to achieve energy savings in servomotor systems. By analyzing the quasi-convex characteristics of the energy-optimal cost function, they developed a computationally efficient parameter tuning algorithm.

To further enhance exoskeleton control, researchers have explored various methodologies. Sun et al. proposed an improved fuzzy control strategy, significantly increasing the stability and accuracy of lower limb exoskeletons for gait assistance[5]. Moreover, Srivastava et al. demonstrated that assist-as-needed robotic gait training not only improves treadmill walking but also enhances overground walking abilities, providing substantial benefits for stroke rehabilitation [6].

A bipedal robot platform is employed in this research to replicate human motion, providing a controlled environment for consistent testing and performance assessment of ex-

oskeleton systems [14][15]. To achieve this, we develop a control system for simulating human gait dynamics, using a simplified double pendulum model to represent the human lower limbs and constructing the bipedal robot's dynamic model based on the motion equation.

After verifying the system's stability, the State-Dependent Riccati Equation (SDRE) control method is applied, offering a theoretically optimal control approach derived from simulation results. This approach leverages the dynamic characteristics of the robot platform to ensure precision in torque control, closely aligning with the intended replication of human motion.

SDRE has been widely applied in constrained system control problems, demonstrating its effectiveness in nonlinear control scenarios [9]. Given the importance of precise and stable control in exoskeleton-assisted walking, this study adopts the SDRE-based control strategy, utilizing a bipedal robot platform to systematically evaluate exoskeleton performance under controlled and repeatable conditions.

Considering the computational requirements of real-time control and hardware torque limitations, an optimal parameterization control method is applied based on a piecewise linear angular velocity model, using the error between the results of SDRE control and the parameterized control as a cost function. This method specifically accounts for the motor's operational speed model, ensuring that angular velocity commands align with the motor's performance characteristics, thereby enhancing the precision and execution efficiency of the control inputs. Consequently, this approach derives optimal control commands for the bipedal robot platform to accurately replicate human motion.

II. LOWER LIMB MODELING AND SDRE CONTROL

A. Dynamic Model

The lower limb model in Figure 1 represents the behavior of the bipedal robot's legs, which is simplified to focus on a single leg for analytical purposes. In the simplification of the model, several key assumptions were adopted to focus on the dynamics and reduce computational complexity. Joint movements are confined to a single dimension, concentrating solely on the primary plane of motion to simplify the equations. The mass of the thigh and lower leg is assumed to be uniformly distributed, allowing for the concentration of mass at the center of mass, which simplifies dynamic calculations. The model considers only the hip and knee joints, excluding the influence of other joints to focus on the principal joints involved in movement. Friction between components is neglected, with attention given only to the primary driving forces and torques. These assumptions facilitate a more straightforward analysis and control of the model while retaining essential dynamic characteristics, aiding in the development of effective control strategies.

To describe the dynamic model of the bipedal robot, P_1 and P_2 denote the joints, and P_{c1} and P_{c2} denote the centers of mass of the thigh and lower leg, respectively. The variables l_1 and l_2 represent the lengths of the thigh and lower leg. Masses of the servo motors are represented by m_1 and m_2 ,

while m_{c1} and m_{c2} represent the masses of the thigh and lower leg.

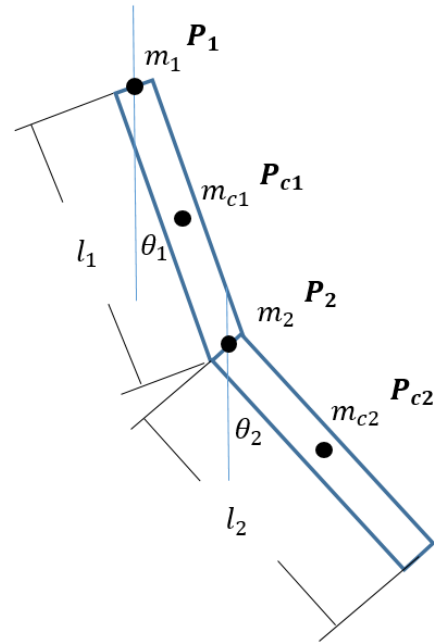


Fig. 1: Dynamic Model of the Lower Limb

TABLE I: DESCRIPTION OF THE PARAMETERS IN THE DYNAMIC MODEL OF THE LOWER LIMB

Symbol	Description
P_1	Hip joint
P_2	Knee joint
P_{c1}	Center of mass of thigh
P_{c2}	Center of mass of lower leg
l_1	Thigh length
l_2	Lower leg length
m_1	Mass of hip servo motor
m_2	Mass of knee servo motor
m_{c1}	Mass of thigh
m_{c2}	Mass of lower leg
θ_1	Hip joint angle
θ_2	Knee joint angle

In the model, we define the angles of the hip and knee as θ_1, θ_2 , corresponding servo motor torques are τ_1, τ_2 . According to the Euler-Lagrange equation:

$$\frac{d}{dt} \left(\frac{\partial L}{\partial \dot{\theta}} \right) - \frac{\partial L}{\partial \theta} = \tau(t) \quad (1)$$

where L is the Lagrangian of the system, defined as the difference between the kinetic energy T and the potential energy V :

$$L = T - V \quad (2)$$

The kinetic energy T can be expressed as:

$$T = \frac{1}{8} m_{c1} l_1^2 \dot{\theta}_1^2 + \frac{1}{2} I_1 \dot{\theta}_1^2 + \frac{1}{2} m_2 l_1^2 \dot{\theta}_1^2 + \frac{1}{2} m_{c2} \left[l_1^2 \dot{\theta}_1^2 + \frac{1}{4} l_2^2 \dot{\theta}_2^2 + l_1 l_2 \dot{\theta}_1 \dot{\theta}_2 \cos(\theta_1 - \theta_2) \right] + \frac{1}{2} I_2 \dot{\theta}_2^2 \quad (3)$$

where I_{c1} and I_{c2} are inertia moments

$$\begin{aligned} I_{c1} &= \frac{1}{12}m_{c1}l_1^2 \\ I_{c2} &= \frac{1}{12}m_{c2}l_2^2 \end{aligned} \quad (4)$$

while the potential energy V :

$$\begin{aligned} V &= -m_2gl_1 \cos \theta_1 - \frac{1}{2}m_{c1}gl_1 \cos \theta_1 \\ &\quad -m_{c2}gl_1 \cos \theta_1 - \frac{1}{2}m_{c2}gl_2 \cos \theta_2 \end{aligned} \quad (5)$$

Substituting these into the Euler-Lagrange equation gives us the equations of motion and express in matrix form:

$$\boldsymbol{\tau} = \mathbf{M}(\boldsymbol{\theta})\ddot{\boldsymbol{\theta}} + \mathbf{V}(\boldsymbol{\theta}, \dot{\boldsymbol{\theta}})\dot{\boldsymbol{\theta}} + \mathbf{G}_{sd}(\boldsymbol{\theta})\boldsymbol{\theta} \quad (6)$$

The matrices $\mathbf{M}(\boldsymbol{\theta})$, $\mathbf{G}_{sd}(\boldsymbol{\theta})$, and $\mathbf{V}(\boldsymbol{\theta}, \dot{\boldsymbol{\theta}})$ are defined as follows:

$$\begin{aligned} \mathbf{M}(\boldsymbol{\theta}) &= \\ &\begin{bmatrix} \frac{1}{4}m_{c1}l_1^2 + I_{c1} + m_2l_1^2 + m_{c2}l_1^2 & \frac{1}{2}m_{c2}l_1l_2 \cos(\theta_1 - \theta_2) \\ \frac{1}{2}m_{c2}l_1l_2 \cos(\theta_1 - \theta_2) & \frac{1}{4}m_{c2}l_2^2 + I_{c2} \end{bmatrix} \end{aligned} \quad (7)$$

$$\begin{aligned} \mathbf{V}(\boldsymbol{\theta}, \dot{\boldsymbol{\theta}}) &= \\ &\begin{bmatrix} 0 & \frac{1}{2}m_{c2}l_1l_2 \sin(\theta_1 - \theta_2)\dot{\theta}_2 \\ -\frac{1}{2}m_{c2}l_1l_2 \sin(\theta_1 - \theta_2)\dot{\theta}_1 & 0 \end{bmatrix} \end{aligned} \quad (8)$$

$$\begin{aligned} \mathbf{G}_{sd}(\boldsymbol{\theta}) &= \\ &\begin{bmatrix} (m_2gl_1 + \frac{1}{2}m_{c1}gl_1 + m_{c2}gl_1) \frac{\sin \theta_1}{\theta_1} & 0 \\ 0 & \frac{1}{2}m_{c2}gl_2 \frac{\sin \theta_2}{\theta_2} \end{bmatrix} \end{aligned} \quad (9)$$

The vectors $\ddot{\boldsymbol{\theta}} = [\ddot{\theta}_1, \ddot{\theta}_2]^T$, $\dot{\boldsymbol{\theta}} = [\dot{\theta}_1, \dot{\theta}_2]^T$, and $\boldsymbol{\theta} = [\theta_1, \theta_2]^T$ in \mathbb{R}^2 denote the angular acceleration, angular velocity, and angles of the bipedal robot motors, respectively. In the matrix $\mathbf{G}_{sd}(\boldsymbol{\theta})$, the fraction term $\frac{\sin \theta}{\theta}$ tends to 1 as θ tends to 0, avoiding singularity.

To facilitate the control and analysis of the bipedal robot system, consider a desired motion profile comprising desired torque, angular acceleration, angular velocity, and motor angles. This profile satisfies the following dynamic equation:

$$\boldsymbol{\tau}_d = \mathbf{M}(\boldsymbol{\theta}_d)\ddot{\boldsymbol{\theta}}_d + \mathbf{V}(\boldsymbol{\theta}_d, \dot{\boldsymbol{\theta}}_d)\dot{\boldsymbol{\theta}}_d + \mathbf{G}_{sd}(\boldsymbol{\theta}_d)\boldsymbol{\theta}_d \quad (10)$$

By subtracting (10) from (6), the error dynamics can be obtained as:

$$\begin{aligned} \boldsymbol{\tau} - \boldsymbol{\tau}_d &= \mathbf{M}(\boldsymbol{\theta})\ddot{\boldsymbol{\theta}} - \mathbf{M}(\boldsymbol{\theta}_d)\ddot{\boldsymbol{\theta}}_d + \mathbf{V}(\boldsymbol{\theta}, \dot{\boldsymbol{\theta}})\dot{\boldsymbol{\theta}} - \mathbf{V}(\boldsymbol{\theta}_d, \dot{\boldsymbol{\theta}}_d)\dot{\boldsymbol{\theta}}_d \\ &\quad + \mathbf{G}_{sd}(\boldsymbol{\theta})\boldsymbol{\theta} - \mathbf{G}_{sd}(\boldsymbol{\theta}_d)\boldsymbol{\theta}_d \end{aligned} \quad (11)$$

Rewrite formula (11)

$$\begin{aligned} \boldsymbol{\tau} - \boldsymbol{\tau}_d &= \mathbf{M}(\boldsymbol{\theta})(\ddot{\boldsymbol{\theta}} - \ddot{\boldsymbol{\theta}}_d) + \mathbf{V}(\boldsymbol{\theta}, \dot{\boldsymbol{\theta}})(\dot{\boldsymbol{\theta}} - \dot{\boldsymbol{\theta}}_d) \\ &\quad + \mathbf{G}_{sd}(\boldsymbol{\theta})(\boldsymbol{\theta} - \boldsymbol{\theta}_d) + \mathbf{g}_f(\boldsymbol{\theta}, \boldsymbol{\theta}_d, \dot{\boldsymbol{\theta}}, \dot{\boldsymbol{\theta}}_d, \ddot{\boldsymbol{\theta}}, \ddot{\boldsymbol{\theta}}_d) \end{aligned} \quad (12)$$

where

$$\begin{aligned} \mathbf{g}_f &= (\mathbf{M}(\boldsymbol{\theta}) - \mathbf{M}(\boldsymbol{\theta}_d))\ddot{\boldsymbol{\theta}}_d \\ &\quad + (\mathbf{V}(\boldsymbol{\theta}, \dot{\boldsymbol{\theta}}) - \mathbf{V}(\boldsymbol{\theta}_d, \dot{\boldsymbol{\theta}}_d))\dot{\boldsymbol{\theta}}_d \\ &\quad + (\mathbf{G}_{sd}(\boldsymbol{\theta}) - \mathbf{G}_{sd}(\boldsymbol{\theta}_d))\boldsymbol{\theta}_d \end{aligned} \quad (13)$$

To control and analyze the error dynamic system, the equations of motion are expressed in a state-space form. State error is defined as $\mathbf{x} = [\boldsymbol{\theta} - \boldsymbol{\theta}_d, \dot{\boldsymbol{\theta}} - \dot{\boldsymbol{\theta}}_d, \boldsymbol{\zeta}]^T$, where $\boldsymbol{\zeta}$ is a variable designed to handle the \mathbf{g}_f term in the dynamic system. The control error vector $\mathbf{u} = \boldsymbol{\tau} - \boldsymbol{\tau}_d \in \mathbb{R}^2$ represents the error between the current torque and the desired torque applied by the servo motors. Reformulating the dynamics yields the state-space representation:

$$\dot{\mathbf{x}} = \mathbf{A}(\mathbf{x})\mathbf{x} + \mathbf{B}(\mathbf{x})\mathbf{u} \quad (14)$$

with observer

$$\mathbf{y} = \mathbf{C}\mathbf{x} \quad (15)$$

where $\mathbf{C} = \mathbf{I}_2 \in \mathbb{R}^{2 \times 2}$ is an elementary matrix.

Rewrite error of state $\mathbf{x} = [x_1, x_2, x_3, x_4, x_5]^T$, and denote $\mathbf{x}_\theta = [x_1, x_2]^T$, $\mathbf{x}_w = [x_3, x_4]^T$, the state-dependent matrices $\mathbf{A}(\mathbf{x}), \mathbf{B}(\mathbf{x})$ are defined by

$$\mathbf{A}(\mathbf{x}) = \begin{bmatrix} \mathbf{0} & \mathbf{I}_2 & \mathbf{0} \\ -\mathbf{M}^{-1}\mathbf{G}_{sd} & -\mathbf{M}^{-1}\mathbf{V} & -\mathbf{M}^{-1}\mathbf{g}_f \\ \mathbf{0} & \mathbf{0} & -\eta \end{bmatrix} \in \mathbb{R}^{5 \times 5} \quad (16)$$

where $\mathbf{M} = \mathbf{M}(\mathbf{x}_\theta + \boldsymbol{\theta}_d)$, $\mathbf{V} = \mathbf{V}(\mathbf{x}_\theta + \boldsymbol{\theta}_d, \mathbf{x}_w + \dot{\boldsymbol{\theta}}_d)$, $\mathbf{G}_{sd} = \mathbf{G}_{sd}(\mathbf{x}_\theta + \boldsymbol{\theta}_d)$

$$\mathbf{B}(\mathbf{x}) = \begin{bmatrix} \mathbf{0} \\ \mathbf{M}^{-1}(\boldsymbol{\theta}) \\ \mathbf{0} \end{bmatrix} \in \mathbb{R}^{5 \times 2} \quad (17)$$

where $\eta > 0$ is a user-decided parameter.

Each leg is modeled independently, and the overall system behavior is determined by combining the dynamics of both legs, taking into account their interactions and coordination during walking or other movements.

To effectively control the bipedal robot platform, the established dynamic model is essential. In the following section, we introduce the State-Dependent Riccati Equation (SDRE) method, which will be used to derive the control strategy based on the developed dynamic model.

B. SDRE Controller

State-Dependent Riccati Equation (SDRE) control is a well-known method used in the control of nonlinear systems. In pursuit of achieving optimal control, it is essential to define a quadratic cost function that captures the performance of the system's states and control inputs over time. In the SDRE framework, this cost function is typically expressed as:

$$J = \int_0^\infty (\mathbf{x}(t)^T \mathbf{Q}\mathbf{x}(t) + \mathbf{u}(t)^T \mathbf{R}\mathbf{u}(t)) dt \quad (18)$$

where $\mathbf{Q}(\mathbf{x})$ and $\mathbf{R}(\mathbf{x})$ are state-dependent weighting matrices. \mathbf{Q} is the state error weighting matrix, which is a semi-positive definite matrix denoted as $\mathbf{Q} \succeq 0$, while \mathbf{R} is the control cost weighting matrix, which is a positive definite matrix denoted as $\mathbf{R} \succ 0$.

For our control design, we assume that these matrices are constant, denoted as $\mathbf{Q}(\mathbf{x}) = \mathbf{Q}$ and $\mathbf{R}(\mathbf{x}) = \mathbf{R}$. Here, the choice of these matrices directly impacts the stability and performance of the control system. Utilizing fixed \mathbf{Q} and \mathbf{R}

matrices is a common practice in applications to simplify the design or ensure system stability.

To find the optimal control law, consider the state-dependent Riccati equation:

$$\mathbf{P}(\mathbf{x})\mathbf{A}(\mathbf{x}) + \mathbf{A}(\mathbf{x})^T\mathbf{P}(\mathbf{x}) - \mathbf{P}(\mathbf{x})\mathbf{B}(\mathbf{x})\mathbf{R}^{-1}\mathbf{B}(\mathbf{x})^T\mathbf{P}(\mathbf{x}) + \mathbf{Q} = 0 \quad (19)$$

where $\mathbf{P}(\mathbf{x})$ is the state-dependent positive definite solution to the Riccati equation. Once the symmetric positive-definite matrix $\mathbf{P}(\mathbf{x})$ is obtained, the optimal control law can be evaluated as:

$$\mathbf{u} = -\mathbf{R}^{-1}\mathbf{B}(\mathbf{x}(t))^T\mathbf{P}(\mathbf{x}(t))\mathbf{x}(t) \quad (20)$$

This control law ensures that the control input $\mathbf{u}(t)$ is applied in such a way that it minimizes the cost function J , leading to optimal performance of the system.

To implement the SDRE controller, the existence and stability of the solution \mathbf{P} for the algebraic Riccati equation can be ensured by checking the stabilizability and detectability of the dynamic system (14)-(17). Hautus Lemma [10] gives the equivalent conditions for stabilizability and detectability.

Theorem 1: The pair (\mathbf{A}, \mathbf{B}) is stabilizable for matrices \mathbf{A}, \mathbf{B} in (16)(17).

Proof: Let $\mathbf{w} = [w_1, w_2, w_3, w_4, w_5]^T$, assume $\mathbf{w}^T\mathbf{B} = \mathbf{0}$ and $\mathbf{w}^T\mathbf{A} = \lambda\mathbf{w}^T$, want to prove that \mathbf{w} must be zero. According to the form of \mathbf{B} in (17)

$$\mathbf{w}^T\mathbf{B} = \mathbf{w}^T \begin{bmatrix} \mathbf{0} \\ \mathbf{M}^{-1} \\ \mathbf{0} \end{bmatrix} = [w_3, w_4]\mathbf{M}^{-1} = [0, 0] \quad (21)$$

Consider

$$\mathbf{w}^T\mathbf{A} = \mathbf{w}^T \begin{bmatrix} \mathbf{0} & \mathbf{I} & \mathbf{0} \\ -\mathbf{M}^{-1}\mathbf{G}_{sd} & -\mathbf{M}^{-1}\mathbf{V} & -\mathbf{M}^{-1}\mathbf{g}_f \\ \mathbf{0} & \mathbf{0} & -\eta \end{bmatrix} \quad (22)$$

Since the left block column and right block column are:

$$\begin{aligned} \mathbf{w}^T \begin{bmatrix} \mathbf{0} \\ -\mathbf{M}^{-1}\mathbf{G}_{sd} \\ \mathbf{0} \end{bmatrix} &= -[w_3, w_4]\mathbf{M}^{-1}\mathbf{G}_{sd} = [0, 0] \\ \mathbf{w}^T \begin{bmatrix} \mathbf{I} \\ -\mathbf{M}^{-1}\mathbf{V} \\ \mathbf{0} \end{bmatrix} &= [w_1, w_2] - [w_3, w_4]\mathbf{M}^{-1}\mathbf{V} = [w_1, w_2] \\ \mathbf{w}^T \begin{bmatrix} \mathbf{0} \\ -\mathbf{M}^{-1}\mathbf{g}_f \\ -\eta \end{bmatrix} &= -\eta w_5 \end{aligned} \quad (23)$$

and by the assumption that $\mathbf{w}^T\mathbf{A} = \lambda\mathbf{w}^T$, we have

$$\begin{aligned} \mathbf{w}^T\mathbf{A} &= [0, 0, w_1, w_2, -\eta w_5] \\ &= [\lambda w_1, \lambda w_2, \lambda w_3, \lambda w_4, \lambda w_5] \end{aligned} \quad (24)$$

The first two components of $\mathbf{w}^T\mathbf{A}$ leads to 2 possible cases

- 1) $\lambda = 0$
- 2) $[w_1, w_2] = [0, 0]$

Since case 1 leads to the result that $[w_1, w_2] = [0, 0]$, we only need to consider case 2. For case 2, to show that $\mathbf{w} = \mathbf{0}$, we have

$$[\lambda w_1, \lambda w_2, \lambda w_3, \lambda w_4, \lambda w_5] = [0, 0, 0, 0, -\eta w_5] \quad (25)$$

Note that $\eta > 0$ is a parameter chosen by user, and $Re(\lambda) > 0$ is the assumption [10]. Therefore, the equality $\lambda w_5 = -\eta w_5$ holds only if $w_5 = 0$ and it implies that $\mathbf{w} = \mathbf{0}$. ■

Theorem 2: The pair (\mathbf{A}, \mathbf{C}) is detectable for matrices \mathbf{A}, \mathbf{C} in (15)(16).

For the detectability, according to equation of observation (15), \mathbf{C} is elementary matrix in the system. It is straightforward to show that the pair (\mathbf{A}, \mathbf{C}) is detectable.

Theorem 3: Suppose that (\mathbf{A}, \mathbf{B}) is stabilizable and (\mathbf{A}, \mathbf{C}) is detectable. Then the Riccati equation in (19) has a unique positive semi-definite solution \mathbf{P} . Moreover, $(\mathbf{A} - \mathbf{B}\mathbf{R}^{-1}\mathbf{B}^T\mathbf{P})$ is stable.

By Theorem 3 in [7], algebraic Riccati equation (19) has unique solution \mathbf{P} such that the dynamic system is stable with control rule (20)

$$\begin{aligned} \dot{\mathbf{x}} &= \mathbf{A}\mathbf{x} + \mathbf{B}\mathbf{u} \\ &= \mathbf{A}\mathbf{x} + \mathbf{B}(-\mathbf{R}^{-1}\mathbf{B}^T\mathbf{P})\mathbf{x} \\ &= (\mathbf{A} - \mathbf{B}\mathbf{R}^{-1}\mathbf{B}^T\mathbf{P})\mathbf{x} \end{aligned} \quad (26)$$

Through the proof of stabilizability and the statement of Theorem 3, we ensure the stability of the dynamic system of the lower limb bipedal robot platform. However, one of the challenges in implementing SDRE controllers is the computational complexity involved, particularly when dealing with real-time applications. To address this issue, the next section introduces a parameterization technique aimed at improving computational efficiency. By simplifying the control method, we streamline the computation process, making it more practical for real-time servo motor control.

III. CONTROL PARAMETERIZATION METHOD

In this section, we will delve into the overall process of utilizing parameterized angular velocity and angular acceleration to approximate human motion profile.

To effectively parameterize, we focus on selecting appropriate nodes. In previous approaches [14], human motion was simulated by moving the joints of a bipedal robot to specific angles at designated times. This time, after the desired path is given, we select feature times from the measured human motion angle profile $\boldsymbol{\theta}(t)$ and separate it into several sub-intervals based on the curvature extrema of the target motion. At the time when curvature extrema occur, it indicates that the joints are activating, deactivating, or changing the direction of motion. These significant changes in human motion provide reference points for the control system to send new commands to the servo motors. Within each time segment defined by the nodes, the target angular velocity $\boldsymbol{\omega}$ and angular acceleration $\boldsymbol{\alpha}$ are parameterized using a trapezoidal ramping model.

This model focus only on the significant changes in the motion trajectory and reducing the complexity of the calculations. Only one acceleration parameter is needed per interval, reflecting the two-phase dynamics of the motion: an initial phase of linear acceleration, followed by a subsequent phase of constant velocity. Equation (27) defines the angular

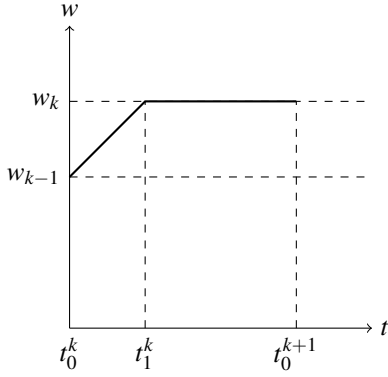


Fig. 2: Piecewise linear representation is applied to simplify the motor control commands by focusing on significant changes in the motion trajectory.

acceleration α_k within the time interval $[t_0^k, t_1^k]$:

$$\alpha_k := \frac{w_k - w_{k-1}}{t_1^k - t_0^k} \quad (27)$$

where w_{k-1} represents the initial angular velocity at the start of the k -th time interval, and w_k is the target angular velocity at the end of this interval. t_1^k is not a predetermined node but rather a parameter that will be implicitly optimized, determining the point at which the velocity transitions from w_{k-1} to w_k .

Suppose a human motion profile $\theta(t)$ lies within the time interval $[0, T]$, and a sequence of characteristic times $\{t_0^i\}_{i=1}^n$ ($t_0^1 = 0, t_0^n = T$) is pre-defined based on the second derivative of $\theta(t)$. Within each subinterval $[t_0^k, t_0^{k+1}]$ for $k = 1, 2, \dots, n-1$, the servo motor reaches the speed parameter w_k with acceleration parameter α_k . The expression of this approximation is given as a function of t in (28). The parameters w_k, α_k are bounded by the motor's physical speed and acceleration constraints as shown in (29).

The piecewise linear velocity profile can be expressed as:

$$\tilde{w}(t) = \begin{cases} w_{k-1} + \alpha_k(t - t_0^k), & \text{for } t_0^k \leq t \leq t_1^k, \\ w_k, & \text{for } t_1^k < t \leq t_0^{k+1}. \end{cases} \quad (28)$$

where the parameters w_k and α_k must satisfy the motor's physical constraints:

$$\begin{aligned} w_{min} \leq w_k \leq w_{max}, & \quad \text{for } k = 1, \dots, n, \\ \alpha_{min} \leq \alpha_k \leq \alpha_{max}, & \quad \text{for } k = 1, \dots, n. \end{aligned} \quad (29)$$

Equation (30) represents the angular velocities w_k and the acceleration parameters α_k for each segment, combining them into vector forms \mathbf{w} and $\boldsymbol{\alpha}$, respectively.

$$\begin{aligned} \mathbf{w} &:= [w_1, \dots, w_n]^T \\ \boldsymbol{\alpha} &:= [\alpha_1, \dots, \alpha_n]^T \end{aligned} \quad (30)$$

Since the approximations angle profile $\tilde{\theta}(t)$ can be obtained by integrating (28). We have the optimization problem:

$$(\mathbf{w}^*, \boldsymbol{\alpha}^*) = \arg \min_{\mathbf{w}, \boldsymbol{\alpha}} J(t; \mathbf{w}, \boldsymbol{\alpha}) \quad (31)$$

subject to

$$\begin{aligned} w_{min} \leq w_k \leq w_{max} & \quad \text{for } k = 1, \dots, n \\ \alpha_{min} \leq \alpha_k \leq \alpha_{max} & \quad \text{for } k = 1, \dots, n \end{aligned} \quad (32)$$

where the cost function is

$$J(t; \mathbf{w}, \boldsymbol{\alpha}) = \left(\frac{1}{T} \int_0^T \mathbf{e}(t; \mathbf{w}, \boldsymbol{\alpha})^T \mathbf{W} \mathbf{e}(t; \mathbf{w}, \boldsymbol{\alpha}) dt \right)^{\frac{1}{2}} \quad (33)$$

the approximation error $\mathbf{e}(t; \mathbf{w}, \boldsymbol{\alpha}) = \boldsymbol{\tau} - \tilde{\boldsymbol{\tau}}$, where the estimation of torque $\tilde{\boldsymbol{\tau}}$ is obtained by (6) with estimated $\tilde{\boldsymbol{\theta}}, \tilde{\mathbf{w}}, \tilde{\boldsymbol{\alpha}}$, and the diagonal matrix $\mathbf{W} \in \mathbb{R}^{2 \times 2}$ is the weight matrix.

These expressions can be used in MATLAB with commands like `fmincon` to find the appropriate motor command sequences, which can then be applied through motor control programs to reproduce human motion.

IV. EXPERIMENT

The proposed bipedal robot platform is designed with four degrees of freedom (DOFs), which correspond to the left/right knee joints and the left/right hip joints. Each DOF is equipped with an actuator and an inertial measurement unit (IMU), providing real-time information on joint angles, angular velocity. The mechanical structure of the platform consists of a steel frame and a fixed hanger to simulate the biomechanical properties of the lower limbs, following the design principles described in [14] [15]. To facilitate comparative testing with the exoskeleton, 3D-printed leg profiles were created, allowing the exoskeleton to be worn on the platform for experiments. The control and data acquisition system (CADAS) is responsible for signal transmission and data processing. The CADAS consists of a microcontroller, an I2C multiplexer, and IMUs, and it handles the transmission of joint data from the bipedal robot to the user end through RS485 and USB interfaces. This architecture enables the testing and analysis of the exoskeleton's performance when mounted on the bipedal robot platform.

To validate the accuracy of the proposed method, we conducted a series of motion evaluations, which aimed to compare the states of the joints in both legs and observe the resulting torque output. In these experiments, the parameters in TABLE I are

$$l_1 = 0.251 \text{ m}, \quad l_2 = 0.28 \text{ m}, \quad m_1 = 0.876 \text{ kg},$$

$$m_2 = 0.876 \text{ kg}, \quad m_{c1} = 2.89 \text{ kg}, \quad m_{c2} = 3.242 \text{ kg}.$$

and weight matrix \mathbf{W} is set as:

$$\mathbf{W} = \begin{bmatrix} 10 & 0 \\ 0 & 10 \end{bmatrix}$$

To validate the accuracy of the control method for the bipedal robot proposed in this thesis, a comparison was made with the SDRE method simulated in MATLAB. Weight matrix \mathbf{Q}, \mathbf{R} in SDRE cost function (18) is set as:

$$\mathbf{Q} = \begin{bmatrix} 500 & 0 & 0 & 0 & 0 \\ 0 & 500 & 0 & 0 & 0 \\ 0 & 0 & 20 & 0 & 0 \\ 0 & 0 & 0 & 20 & 0 \\ 0 & 0 & 0 & 0 & 1 \end{bmatrix}$$

$$R = \begin{bmatrix} 20 & 0 \\ 0 & 20 \end{bmatrix}$$

Both methods were applied to reproduce the same set of human motion data, and the RMSE was calculated against the original human motion data. The comparison results are shown in Table II.

TABLE II: Comparison of RMSE in motion angles for SDRE and bipedal robot relative to human motion.

Motion	Side	Part	RMSE of SDRE(°)	RMSE of bipedal Robot(°)
Squat	Left	Hip	0.2485	5.3367
Squat	Left	Knee	0.3240	3.0977
Squat	Right	Hip	0.2622	5.6638
Squat	Right	Knee	0.3228	1.3157
Walk	Left	Hip	0.3344	5.3188
Walk	Left	Knee	0.4005	4.9988
Walk	Right	Hip	0.3260	5.2775
Walk	Right	Knee	0.3992	4.3366

Figure 3 and Figure 4 show the torque results obtained from the two methods. In Figure 3, the red line represents the torque of the right hip and knee during human motion, while the blue dashed line represents the torque when the bipedal robot platform reproduces the human motion. In Figure 4, the red line again represents the torque during human motion, while the blue dashed line shows the torque results of SDRE simulation.

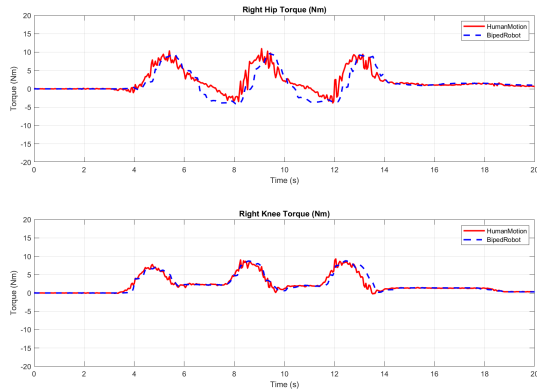


Fig. 3: Torque of the right hip/knee joint with proposed method

V. CONCLUSIONS

In this study, we demonstrated a high degree of motion reproducibility by leveraging pre-recorded human movement data combined with offline optimization. This approach enables the precise replication of the wearer's natural movements, ensuring high-fidelity motion reproduction. Furthermore, system stability was significantly improved through offline optimization calculations, which circumvent the limitations of real-time processing. As a result, optimized speed commands and timing can be consistently applied to the bipedal robot platform after multiple rounds of refinement.

The system offers ample flexibility for adjustments, as the offline nature of the optimization process allows for

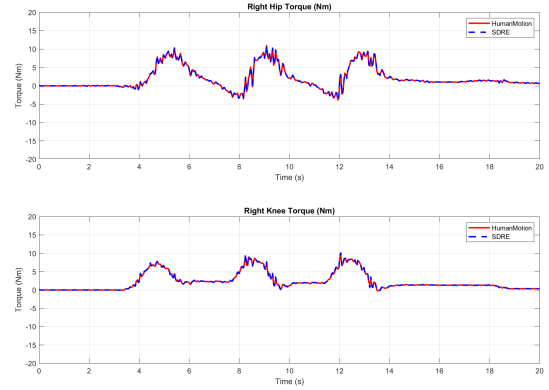


Fig. 4: Torque of the hip/knee joint with SDRE method

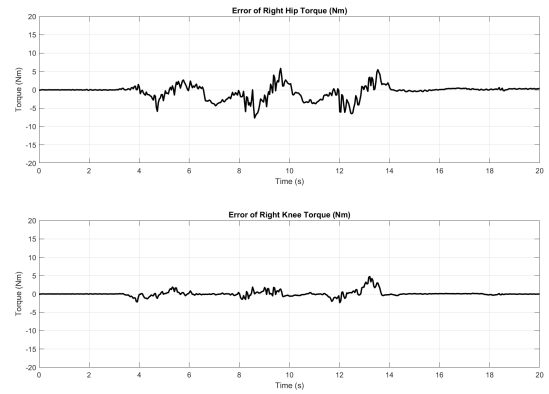


Fig. 5: Torque error of the right hip/knee joint with proposed method

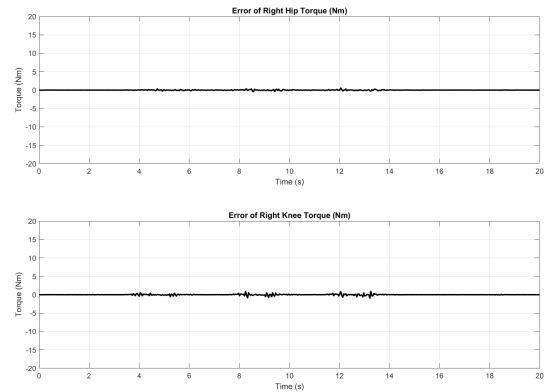


Fig. 6: Torque error of the hip/knee joint with SDRE method

repeated parameter tuning without interrupting real-time system operation. This not only facilitates the discovery of optimal control solutions but also reduces the computational burden during runtime. By offloading the majority of the computational tasks to an offline environment, the real-time controller experiences reduced processing load, leading to enhanced execution efficiency in live control scenarios.

References are important to the reader; therefore, each citation must be complete and correct. If at all possible, references should be commonly available publications.

REFERENCES

- [1] B.-K. Lee, H.-D. Lee, J.-Y. Lee, K. Shin, J.-S. Han, and C.-S. Han, "Development of dynamic model-based controller for upper limb exoskeleton robot," in *2012 IEEE International Conference on Robotics and Automation*, 2012, pp. 3173–3178. doi: 10.1109/ICRA.2012.6224675.
- [2] D. Sanz-Merodio, M. Cestari, J.C. Arevalo, and E. Garcia, "Control Motion Approach of a Lower Limb Orthosis to Reduce Energy Consumption," in *International Journal of Advanced Robotic Systems*, 2012. doi: 10.5772/51903.
- [3] F. Chen, Y. Yu, Y. Ge, and Y. Fang, "WPAL for human power assist during walking using dynamic equation," in *2009 International Conference on Mechatronics and Automation*, 2009, pp. 1039–1043. doi: 10.1109/ICMA.2009.5246270.
- [4] N. L. Tagliamonte, F. Sergi, G. Carpino, D. Accoto, and E. Guglielmelli, "Human-robot interaction tests on a novel robot for gait assistance," in *2013 IEEE 13th International Conference on Rehabilitation Robotics (ICORR)*, 2013, pp. 1–6. doi: 10.1109/ICORR.2013.6650387.
- [5] W. Sun, J.-W. Lin, S.-F. Su, N. Wang, and M. J. Er, "Reduced Adaptive Fuzzy Decoupling Control for Lower Limb Exoskeleton," *IEEE Transactions on Cybernetics*, vol. 51, no. 3, pp. 1099–1109, 2021. doi: 10.1109/TCYB.2020.2972582.
- [6] S. Srivastava, P.-C. Kao, S. H. Kim, P. Stegall, D. Zanutto, J. S. Higgenson, S. K. Agrawal, and J. P. Scholz, "Assist-as-Needed Robot-Aided Gait Training Improves Walking Function in Individuals Following Stroke," *IEEE Transactions on Neural Systems and Rehabilitation Engineering*, vol. 23, no. 6, pp. 956–963, 2015. doi: 10.1109/TNSRE.2014.2360822.
- [7] K. Zhou and J. C. Doyle, *Essentials of Robust Control*, vol. 104. Upper Saddle River, NJ: Prentice Hall, 1998, pp. 233–244.
- [8] P. J. Antsaklis and A. N. Michel, *Linear Systems*, vol. 8. New York: McGraw-Hill, 1997, pp. 272–274.
- [9] J. R. Cloutier and J. C. Cockburn, "The state-dependent nonlinear regulator with state constraints," in *Proceedings of the 2001 American Control Conference (Cat. No. O1CH37148)*, 2001.
- [10] B. D. O. Anderson and J. B. Moore, *Optimal Control: Linear Quadratic Methods*. Upper Saddle River, NJ: Prentice Hall, 1990.
- [11] Parker Hannifin Corporation, "Servo Fundamentals," Parker Hannifin Corporation, 2010.[Online]. Available: <https://www.parker.com/parkerimages/emn/ServoFundamentals.pdf>.
- [12] H. Shao, D. Liao, and J. W. F. Cheung, "System Identification and Profile Planning for High Accuracy Servo System," in *Intelligent Robotics and Applications (ICIRA 2008)*, C. Xiong et al., Eds., Lecture Notes in Artificial Intelligence, vol. 5314. Springer-Verlag Berlin Heidelberg, 2008, pp. 410–419.
- [13] Z. Yu, C. Han, and H. Mu, "A novel approach of tuning trapezoidal velocity profile for energy saving in servomotor systems," in *Proceedings of the 2015 34th Chinese Control Conference (CCC)*, 2015, pp. 7028–7033. doi: 10.1109/ChiCC.2015.7260775.
- [14] C.-W. Lan, S.-S. Lin, B.-S. Chen, M.-F. Lo, C.-T. Ku, and M.-C. Chien, "Design and Development of a Biped Robot for a Knee Exoskeleton Analysis," in *2021 International Symposium on Intelligent Signal Processing and Communication Systems (ISPACS)*, IEEE, Taoyuan, Taiwan, 2021.
- [15] C. -W. Lan, S. -S. Lin, C. -T. Ku, B. -S. Chen, M. -F. Lo and M. -C. Chien, "Using Biped Robot on Knee Exoskeleton for Stair Climbing Assistance Analysis," *2021 International Automatic Control Conference (CACS)*, Chiayi, Taiwan, 2021, pp. 1-6, doi: 10.1109/CACS52606.2021.9639061.
- [16] R. Fazel, A. M. Shafei, and S. R. Nekoo, "Dynamic modeling and closed-loop control design for humanoid robotic systems: Gibbs–Appell formulation and SDRE approach," *Multibody System Dynamics*, 2024, pp. 1–30.
- [17] S. O. Schrade *et al.*, "Knee Compliance Reduces Peak Swing Phase Collision Forces in a Lower-Limb Exoskeleton Leg: A Test Bench

- Evaluation," *IEEE Transactions on Biomedical Engineering*, vol. 68, no. 2, pp. 535-544, Feb. 2021, doi: 10.1109/TBME.2020.3006787.
- [18] C. A. Laubscher and J. T. Sawicki, "Gait Guidance Control for Damping of Unnatural Motion in a Powered Pediatric Lower-Limb Orthosis," *2019 IEEE 16th International Conference on Rehabilitation Robotics (ICORR)*, Toronto, ON, Canada, 2019, pp. 676-681, doi: 10.1109/ICORR.2019.8779437.
- [19] Y. He, G. Zhou, H. Jiang, and J. Zhang, "Risk management and regulations for lower limb medical exoskeletons: a review," in **Medical Devices: Evidence and Research**, vol. 10, 2017, pp. 89-107.